EUKARYOTIC CELL, Jan. 2005, p. 121–133 Vol. 4, No. 1
1535-9778/05/$08.00+0 doi:10.1128/EC.4.1.121–133.2005

Role for RNA-Binding Proteins Implicated in Pathogenic Development of *Ustilago maydis*†

Philip Becht, Evelyn Vollmeister, and Michael Feldbrügge*

Department for Organismic Interactions, Max Planck Institute for Terrestrial Microbiology, Marburg, Germany

Received 26 August 2004/Accepted 26 October 2004

Ustilago maydis **causes smut disease on corn. Successful infection depends on a number of morphological transitions, such as pheromone-dependent formation of conjugation tubes and the switch to filamentous dikaryotic growth, as well as different types of mycelial structures during growth within the host plant. In order to address the involvement of RNA-binding proteins during this developmental program, we identified 27 open reading frames from the genome sequence encoding potential RNA-binding proteins. They exhibit similarities to RNA-binding proteins with Pumilio homology domains (PUM), the K homology domain (KHD), the double-stranded RNA binding motif (DSRM), and the RNA recognition motif (RRM). For 18 of these genes, we generated replacement mutants in compatible haploid strains. Through analysis of growth behavior, morphology, cyclic AMP response, mating, and pathogenicity, we identified three candidates with aberrant phenotypes. Loss of Khd1, a K homology protein containing three KHDs, resulted in a cold-sensitive growth phenotype. Deletion of *khd4* encoding a protein with five KHDs led to abnormal cell morphology, reduced mating, and virulence. *rrm4*Δ strains were affected in filamentous growth and pathogenicity. Rrm4 is an RRM protein with a so far unique domain organization consisting of three N-terminal RRMs as well as a domain found in the C terminus of poly(A)-binding proteins. These results indicate a role for RNA-binding proteins in regulation of morphology as well as in pathogenic development in *U. maydis*.**

Presently, the causative agent of corn smut disease, *Ustilago maydis*, and the human pathogen *Cryptococcus neoformans* are model systems of choice for pathogenic basidiomycetes (7, 25). For completion of its sexual life cycle, *U. maydis* depends on a number of morphological transitions. These are exquisitely regulated and intimately connected to the presence of its host. A prerequisite for infection is mating of two compatible haploid sporidia that proliferate by budding. Mating involves the formation of conjugation hyphae that grow towards each other and fuse at their tips (59). Upon cell fusion, a dikaryon is generated that arrests its cell cycle and switches to fast polar growth. The dikaryon represents the infective form and is able to penetrate the plant surface after formation of appressorium-like structures. Inside the plant, the cell cycle stop is released, resulting in a multicompartmental dikaryotic mycelium. At later stages karyogamy occurs and diploid teliospores are formed (4, 27).

Mating compatibility is determined by a tetrapolar mating system consisting of two mating-type loci designated *a* and *b*. The biallelic *a* locus (*a1* and *a2*) encodes the precursor and receptor of lipopeptide pheromones regulating intercellular recognition (9). The multiallelic *b* locus encodes a pair of homeodomain proteins, bE and bW, that are only active as heterodimeric transcription factors with subunits derived from different allelic origins (29). The formation of an active bE/bW heterodimer is necessary and sufficient for the developmental switch to fast polar growth. The concerted action of mating-type gene products is orchestrated by cross talk between protein kinase A (PKA) and mitogen-activated protein kinase (MAPK) signaling (17, 36, 54).

To investigate regulation of cell polarity and morphology during pathogenic development, we tested the involvement of RNA-binding proteins, since this class of proteins determines cell polarity in higher eukaryotes during developmental programs such as oogenesis and early embryogenesis in *Drosophila melanogaster* and sex determination in *Caenorhabditis elegans*, as well as mammalian stem cell proliferation (34). RNA-binding proteins regulate mRNA activity at the level of maturation, nuclear export, cytoplasmic localization, stability, and translation (15, 40, 42). A well-studied example is Pumilio from *D. melanogaster*, which recognizes a specific response element in the 3′-untranslated region of *hunchback* mRNA. Thereby translation is repressed, resulting in a protein gradient throughout the embryo that determines the posterior polarity of the embryo (44, 69). Also regarding lower eukaryotes, the number of reports that describe connections between RNA-binding proteins and development is growing. PufA from *Dictyostelium discoideum* is involved in determining sporulation in response to starvation by regulating translation of mRNA encoding the catalytic subunit of PKA (60). Nrd1 and Msa1 are negative regulators of sexual differentiation in *Schizosaccharomyces pombe* (26), and Scp160p regulates mating in *Saccharomyces cerevisiae* by interacting with the heterotrimeric G protein Gpa1p during pheromone-responsive MAPK signaling (22).

To study the function of RNA-binding proteins in *U. maydis*, we chose a combinatorial approach based on bioinformatics and reverse genetics, using the recently released genome se-

* Corresponding author. Mailing address: Max Planck Institute for Terrestrial Microbiology, Department of Organismic Interactions, Karl-von-Frisch-Strasse, 35043 Marburg, Germany. Phone: 49-6421-178602. Fax: 49-6421-178609. E-mail: feldbrue@staff.uni-marburg.de.

† Supplemental material for this article may be found at http://ec.asm.org/.

quence (http://www.broad.mit.edu/annotation/fungi/ustilago_maydis/) and an efficient gene replacement strategy (10, 28). Genes encoding potential RNA-binding proteins can be easily identified due to the presence of at least one RNA-binding domain. In eukaryotes, the majority of RNA-binding domains belong to the following four classes that are well defined on primary, secondary, and tertiary structure: the Pumilio homology domain (PUM), the K homology domain (KHD), the double-stranded RNA-binding domain (DSRM), and the RNA recognition motif (RRM) (12, 41, 49).

The PUM was named after its founding member, Pumilio (69, 73). The domain recognizes RNA sequence specifically and is composed of eight tandem repeats, each ~40 amino acids (aa) in length. Characteristic of these repeats is a core consensus containing aromatic and basic amino acids (70). The KHD was first identified in hnRNP K (heterogeneous nuclear ribonucleoprotein K), a major pre-mRNA-binding protein (58). The domain comprises ~60 aa and contains a characteristic Gly-X-X-Gly loop that grips RNA (38, 45). The double-stranded RNA-binding motif is an ~65-aa domain found in various proteins that bind double-stranded RNAs such as Staufen from *D. melanogaster* or RNase III from *Escherichia coli* (31, 61). The RRM is by far the best-characterized and most widespread domain. At present there are 4,160 proteins with 7,079 domains known (http://smart.embl.de/). The RRM is 90 to 100 aa in length, containing two well-conserved sequences, the RNP1 octamer and the RNP2 hexamer (6, 12). Charged and aromatic side chains of RNP1 and RNP2 are solvent exposed and contact RNA (12).

Here, we describe the identification of 27 open reading frames (ORFs) in *U. maydis* encoding putative RNA-binding proteins of the PUM, KHD, DSRM, and RRM types. A subset of 18 gene replacement mutants were generated and subjected to a detailed phenotypic analysis revealing that KHD and RRM candidates are important for pathogenic development.

MATERIALS AND METHODS

Strains. The *E. coli* K-12 derivatives DH5α (Bethesda Research Laboratories) and Top10 (Invitrogen) were used for cloning purposes. *U. maydis* strains FB1, FB2, UM521, SG200, FBD12-17, and FBD11-7 have been published previously (5, 8).

Bioinformatic analysis. In order to identify PUM-type RNA-binding proteins, the following protein sequences (http://smart.embl-heidelberg.de/smart/do_annotation.pl?DOMAIN=Pumilio&BLAST=DUMMY&EVOLUTION=Show#Evolution) have been compared to the genomic sequence from *U. maydis* (http://www.broad.mit.edu/annotation/fungi/ustilago_maydis/) by using BLAST (2): *S. cerevisiae* (7), Q12221, P47077, P39016, Q07807, P25339, Q04373, and P47135; *S. pombe* (9), Q10238, Q09829, Q92347, O94462, O60059, Q92359, Q9P789, Q9UU76, and O74438; *Neurospora crassa* (2), Q8X035, Q9P6D4; *D. discoideum* (1), Q9Y1J5; *Arabidopsis thaliana* (6), Q9LRZ3, Q9SVZ7, BAB08273, Q95547, Q9SFL0, and Q9LVC3; *H. sapiens* (3), AAG31807, O00234, and AAG31806; *C. elegans* (6), O01322, QZ3191, Q9U2G4, Q09487, Q9N3Q2, and Q9N5M6; and *D. melanogaster* (1), Q9VHH6.

To identify KHD-containing proteins, we used the following protein sequences from the SMART (Simple Modular Architecture Research Tool) database (http://smart.embl-heidelberg.de/smart/do_annotation.pl?DOMAIN=KH&BLAST=DUMMY&EVOLUTION=Show#Evolution): *S. cerevisiae* (6), Q07834, Q12186, YBD2, PBP2, RS3, and Q99216; *S. pombe* (7), O59810, O74359, O74919, O74555, O74777, YAJE_Schpo, and O14044; *N. crassa* (1), Q9P6B5; *H. sapiens* (5), Q13601, AAG02184, AAG45476, Q9Y307, and Vigilin; *C. elegans* (1), Q9U3B2; and *D. melanogaster* (1), Q9V8H6.

In order to identify DSRM-type proteins, we used the following protein sequences (http://smart.embl-heidelberg.de/smart/do_annotation.pl?DOMAIN=DSRM&BLAST=DUMMY&EVOLUTION=Show#Evolution): *S. cerevisiae* (2), RM03 and RNT1; *S. pombe* (2), O43042 and PAC1; *N. crassa* (2), Q7S6N0 and Q9P6D6; and *D. melanogaster* (23), AAQ23615, Q8MRC7, Q8MRY4, Q95YG3, Q960Y4, Q961S7, Q9GNJ2, Q9NHW9, Q9NII2, Q9U6N4, Q9V847, Q9V9V7, Q9VCU9, Q9VHB0, Q9VJY9, Q9VLW8, Q9VRL8, Q9VY45, Q9VZ88, Q9W5S7, Q9XYN5, MLE, and STAU.

To identify RRM-type proteins, we used the following sequences (http://smart.embl-heidelberg.de/smart/do_annotation.pl?DOMAIN=RRM&BLAST=DUMMY&EVOLUTION=Show#Evolution): *S. cerevisiae* (6), P04147, P32588, P38922, P32831, P27476, and P34217; *S. pombe* (2), Q09702 and P08965; *H. sapiens* (3), Q9UNP9, Q15717, and Q9Y3B4; and *D. melanogaster* (5), P19018, P19339, P16914, O02374, and AAF54070.

For the phylogenetic analysis, sequence alignments were performed with CLUSTAL_X (63). Dendrograms were constructed with MEGA 2.1 (http://www.megasoftware.net) (35) with the minimum evolution algorithm and an initial tree obtained by the neighbor-joining method. Two KHD proteins each have been predicted from *C. neoformans* (Cn; http://www.broad.mit.edu/annotation/fungi/cryptococcus_neoformans/) and *Coprinus cinereus* (Cc; http://www.broad.mit.edu/annotation/fungi/coprinus_cinereus/). KHD protein Cn1, 1,113 aa in length, is located on contig 1.77 between nucleotide positions 175691 and 172233. Two introns were predicted (intron 1, 173461 to 1733960; and intron 2, 172828 to 172779). KHD protein Cn2, 891 aa in length, is located on contig 1.12 between nucleotide positions 65877 and 61787. Eight introns were predicted (intron 1, 65225 to 65028; intron 2, 64929 to 64881; intron 3, 64745 to 64107; intron 4, 63950 to 63919; intron 5, 63720 to 63383; intron 6, 62923 to 62877; intron 7, 62675 to 62618; intron 8, 62371 to 62318). KHD protein Cc1, 1,228 aa in length, is located on contig 1.44 between nucleotide positions 260066 and 264281. Seven introns were predicted (intron 1, 260264 to 260745; intron 2, 261695 to 264754; intron 3, 262019 to 262074; intron 4, 262244 to 262303; intron 5, 262418 to 262528; intron 6, 262595 to 262654; intron 7, 263275 to 263334). KHD protein Cc2, 797 aa in length, is located on contig 1.9 between nucleotide positions 41512 and 44651. Eight introns were predicted (intron 1, 41834 to 41904; intron 2, 42041 to 42094; intron 3, 42237 to 42284; intron 4, 42550 to 42610; intron 5, 42821 to 43159; intron 6, 43619 to 43671; intron 7, 43873 to 43920; intron 8, 44306 to 44376).

Generation of gene replacement strains in *U. maydis*. Gene replacement mutants were generated by a PCR-based approach (10, 28). For each gene replacement construct, eight PCR primers were designed: u1, u2, and u3 (upstream flanking sequence); d1, d2, and d3 (downstream flanking sequence); and p1 and p2 (10) (see Fig. 2A and Table 2; see Table S1 in the supplemental material). Primer u3 and d1 introduced SfiI(u) and SfiI(d) recognition sites at the 3′ end of the upstream flank and the 5′ end of the downstream flank, respectively. Initially ~1-kb upstream and downstream flanking sequences of the ORF region of interest were amplified with genomic DNA of wild-type strain UM521 (*a1b1*) as a template and primer combinations u2/u3 and d1/d2, respectively (Fig. 2B, lanes 1 and 2; Table 2). PCR products were cleaved with SfiI and ligated in the presence of a compatible 1.8-kb SfiI(u)/SfiI(d) fragment containing the hygromycin resistance cassette (28). Gel-purified ligation products were inserted in pCR2.1-TOPO (Invitrogen; Table 2, pUMa). The resulting plasmids were used as a template for PCR with primers u2 and d2 (Fig. 2B, lane 3), and the respective products were transformed in *U. maydis* wild-type strains FB1 and FB2 (*a1b1* and *a2b2*, respectively). Hygromycin-resistant colonies were subjected to whole-cell PCR analysis using primers p1 and p2 (Fig. 2B, lanes 4 to 6; Table 2). Amplification of an ~200-bp-long fragment was diagnostic for the presence of the wild-type allele indicative for a nonhomologous integration event (Fig. 2B, lane 4). Only those transformants in which the diagnostic PCR product was absent were analyzed further (Fig. 2B, lanes 5 and 6). Successful gene replacements were verified by detection of an ~1-kb PCR product using primers u1 and hu (Fig. 2B, lanes 7 to 9) and by amplification of ~1-kb PCR products with primer combinations d3 and hd (Fig. 2B, lanes 10 to 12). To validate this approach, we verified successful gene replacements in the cases of *pum1-3*Δ and *khd4*Δ, as well as *rrm4*Δ, by Southern analysis (10).

Growth on CM and minimal medium plates. Starter cultures were grown overnight on a rotary shaker at 220 rpm in liquid complete medium (CM) at 28°C (24). Using a Neubauer counting chamber, cell density was determined. An aliquot of cells was centrifuged at 3,500 rpm (5 min at room temperature), and the density of cells was adjusted to 10^6 cells/ml with sterile water. Two-microliter cell suspensions of fivefold serial dilutions were applied as spots in six steps on CM or nitrate minimal (NM) plates (3-g/liter KNO_3, 10-g/liter glucose, and 2-g/liter agarose) (24). Plates were incubated for 2 to 5 days at 15, 28, and 34°C. Pigmentation, morphology, and growth of colonies were scored by visual inspection.

Measuring doubling time during exponential growth. Starter cultures were grown overnight on a rotary shaker at 220 rpm in liquid CM at 28°C (24). A 1-μl

cell suspension of stationary-phase starter cultures was transferred in 1 ml of CM and incubated on a thermomixer compact (Eppendorf) at 400 rpm in a 24-well plate at 28°C. At appropriate time intervals, optical density (OD) was measured as OD_{600} with a TECAN Saphire fluorescence reader. Doubling time was calculated from the slope of a linear regression line derived from values during the exponential phase of growth (see Fig. S1 in the supplemental material).

Quantifying response to external cAMP. Starter cultures (1 ml) were grown overnight on a thermomixer compact (Eppendorf) at 1,100 rpm in liquid CM (24) at 28°C using 2-ml tubes sealed with Lid_{Bac} (Eppendorf). Two-microliter cell suspensions of stationary-phase starter cultures were transferred in 1 ml of CM in the presence or absence of 15 mM cyclic AMP (cAMP) and incubated on a thermomixer compact (Eppendorf) at 1,100 rpm for 18 h at 28°C. An aliquot was transferred to a Neubauer counting chamber, and the percentage of cells in aggregates of more than two cells was counted (for each quantification, ~100 cells; see Fig. S2 in the supplemental material).

Mating, pheromone production, and filamentation assays. Starter cultures were grown overnight on a rotary shaker at 220 rpm in PD medium (2.4% potato dextrose broth; Difco). Stationary-phase cultures were diluted in PD medium to an OD at 600 nm (OD_{600}) of 0.2. After growth at 28°C on a rotary shaker at 220 rpm to an OD_{600} of 0.5, a 0.5-ml aliquot of cell suspension was centrifuged at 3,500 rpm (5 min at room temperature). Cells were resuspended in 0.5 ml of water. For filamentation assays, cells were applied as spots and, for mating as well as pheromone production assays, respective strains were applied as cospots on charcoal-containing PD plates that were sealed with Parafilm and incubated at 22°C for 24 to 48 h.

Cell morphology and conjugation hypha formation. Starter cultures were grown overnight on a rotary shaker at 220 rpm in CM (24) at 28°C. Stationary-phase cultures were diluted in CM to an OD_{600} of 0.2. After incubation as mentioned above to an OD_{600} of 0.5, a 1-ml aliquot of cells was centrifuged at 3,500 rpm (5 min at room temperature) and cells were resuspended in CM with or without synthetic a1 or a2 pheromone dissolved in dimethyl sulfoxide (2.5 μg/ml) (62). Cells were incubated for 5 h at 28°C in a 15-ml plastic tube rotating with 20 rpm. For microscopic observation, we used a Zeiss Axiophot with differential interference contrast optics. Pictures were taken with a charge-coupled device camera (AxioCam HRm; Zeiss).

Pathogenicity assay. Plant infections of corn variety Early Golden Bantam (Olds Seeds, Madison, Wis.) were performed as described previously (11). Tumor formation was scored after 14 days. In the case of *rrm4* deletion mutants, a more detailed disease rating was adopted from earlier studies (20) using the following categories: no tumor, minor disease symptoms at leaves (disease area with tumors is not larger than 1.5 cm and the number of tumors does not exceed a cutoff of 20), major disease symptoms at leaves (disease area with tumors is wider than 1.5 cm and the number of tumors exceeds 20), minor disease symptoms at stems (disease area with tumors is not larger than 4 cm and heights of tumors do not exceed 0.6 cm), major disease symptoms at stems (disease with tumors is larger than 4 cm and heights of tumors exceed 0.6 cm), as well as wilted or dead plants.

RESULTS

Identification of ORFs encoding potential RNA-binding domains of the PUM, KHD, DSRM, and RRM types. In order to identify genes encoding RNA-binding proteins of the PUM, KHD, DSRM, and RRM types in the genome of *U. maydis*, we selected known RNA-binding proteins of the respective types according to the SMART database from fungi and model organisms such as *A. thaliana*, *D. melanogaster*, *C. elegans*, and *H. sapiens* (http://smart.embl.de; accession numbers are given in Materials and Methods) (37, 56). The respective protein sequences were compared to predicted ORFs from *U. maydis* by using BLAST (http://www.broad.mit.edu/annotation/fungi/ustilago_maydis/) (2). Candidate ORFs were analyzed with the SMART service at http://smart.embl.de (37, 56). Only those proteins were considered positive that were predicted to contain the respective domain with scores more significant than established cutoff values (http://smart.embl.de/) (Fig. 1). All ORFs were defined by conceptual translation from the genomic sequence. In four cases, we were able to predict the presence of introns according to sequence similarities to homologous proteins (Table 1). However, the predicted sequences might still contain surplus amino acids due to the presence of in-frame introns.

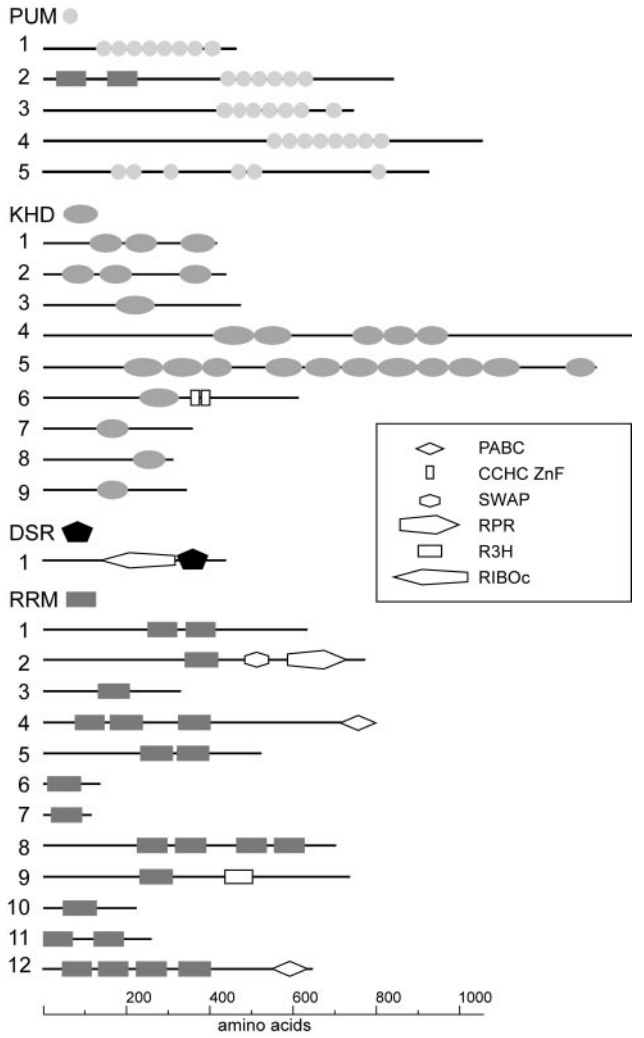

FIG. 1. Domain structures of PUM-, KHD-, DSRM-, and RRM-type RNA-binding proteins. Lines symbolize ORFs (length scale at the bottom), and domains are indicated by symbols. These are either labeled adjacently in cases of PUM, KHD, DSRM (DSR), and RRM (at the top of each class) or are given in the inset. PABC, poly(A)-binding protein C terminus; CCHC ZnF, CCHC-type zinc finger; SWAP, suppressor-of-white-apricot splicing regulator; RPR, regulation of pre-mRNA; R3H, conserved arginine histidine domain; and RIBOc, RNase III family. The numbers on the left correspond to the designations of the respective RNA-binding proteins.

For the identification of PUM-type proteins in *U. maydis*, we chose 35 representative proteins containing Pumilio-like repeats from SMART: 19 from various fungi, 6 from *A. thaliana*, 6 from *C. elegans*, 3 from *H. sapiens*, and Pumilio from *D. melanogaster*. Five candidate ORFs were identified in the *U. maydis* genome, designated *pum1* to *-5*. The respective proteins contain several adjacent Pumilio-like repeats with conserved core sequences in the C-terminal half of the protein. These features are hallmarks for this class of proteins (Fig. 1; Table 1) (70). Pum2 has been predicted to contain two addi-

TABLE 1. RNA-binding proteins in *U. maydis*

Gene	No. of potential RBDs[a]	Length of ORF (aa)	Closest yeast homologue[b]	e value ($< e^{-15}$)[c]	Length of yeast homologue (aa)	Contig[d]	Nucleotide position	Deleted region	Chromosome[k]
pum1	1	467	Puf3p	$7e^{-58}$	879	14	1433–2836	1779–2669	I
pum2	3	845	Jsn1p/Puf1p	$2e^{-52}$	1,091	4	78730–76193	77494–76581	I
pum3	1	748				197	19370–21616	20583–20831	XVIII
pum4	1	1,058	Puf4p	$5e^{-72}$	888	115	115768–118711		n.a.[l]
pum5	1	921				101	44697–47462		n.a.
khd1	3	422	Pbp2p	$4e^{-26}$	413	215	157776–156339[f]	157387–156576	XX
khd2	3	442	Pbp2p	$1e^{-23}$	413	124	7412–6173	7330–6459	X
khd3	1	479				139	71807–70368	71480–70994	XI
khd4	5	1,416				129	47506–43256	46492–45548	X
khd5	11	1,330	Scp160p	$9e^{-42}$	1,222	245	18952–14960		n.a.
khd6	2	614	Ms15p	$2e^{-58}$	476	247	93724–95568		XXIII
khd7	1	364	Krr1p	$1e^{-107}$	316	109	110546–109452		VIII
khd8	1	313	Pno1p	$4e^{-67}$	274	117	28298–27357		IX
khd9	1	347	Rps3p	$9e^{-83}$	240	101	137517–136474		VIII
dsr1	1	444	Mrp13p	$1e^{-24}$	390	103	133224–134558		VII
rrm1	2	638				83	396083–397999	396806–397324	V
rrm2	1	779				124	43778–41439	43133–41881	X
rrm3	1	332				34	72086–73354[g]	72518–73235	II
rrm4	3	792				112	120505–118126[h]	120357–119302	VIII
rrm5	2	525				101	247488–249232[i]	248295–248884	VII
rrm6	1	139				109	85216–84797	85182–84979	VIII
rrm7	1	121				86	175280–175645	175292–175649	VI
rrm8	4	704	Ylp184p	$3e^{-96}$	612	157	28299–26185	27551–26442	XIV
rrm9	1	740	Pin4p	$9e^{-37}$	668	126	64830–62611	64209–63824	X
rrm10	1	228				148	37894–37208	37726–37460	XII
rrm11	2	263				208[e]	732–30560[j]	1468–1463	XVI
rrm12	4	651	Pab1p	$1e^{-132}$	577	117	24758–26713		IX

[a] RNA-binding domain.
[b] Only proteins were listed with BLAST expect value below e^{-15}.
[c] BLAST expect value.
[d] Genomic sequence release 1 (http://www.broad.mit.edu/annotation/fungi/ustilago_maydis/).
[e] Fusion of contig 1.208 with 1.207.
[f] Predicted introns at positions 157314 to 157244 and 157174 to 157077.
[g] Predicted introns at positions 72310 to 72489 and 72745 to 72832.
[h] Frameshift at position 119257, as predicted due to comparison to the sequence from Bayer CropScience.
[i] Predicted introns at positions 248204 to 248343 and 248477 to 248557.
[j] Predicted intron at positions 651 to 585.
[k] According to the sequence project from Bayer CropScience.
[l] Information not available, since these genes were missing in this sequence project.

tional RNA-binding domains of the RRM type in its N terminus. This domain composition is reminiscent of the structure of Pumilio-like proteins Puf1p/Jsn1p and Puf2p from *S. cerevisiae*. Both proteins carry a single RRM domain N terminal to these PUM repeats (48). Pum5 belongs to a group of atypical PUM-type proteins, since it contains six PUM repeats that are not clustered in the C terminus (Fig. 1).

To identify KHD proteins, we chose 21 candidates from SMART: 14 from fungi, 5 from *H. sapiens*, and 1 each from *D. melanogaster* and *C. elegans*. Nine candidate ORFs were found and designated *khd1* to *-9* (Fig. 1; Table 1). Khd1 and Khd2 share the same domain organization consisting of three KHD regions and are similar in sequence to the Pab1p-binding protein Pbp2p that is required for proper chromosome segregation during meiosis (39, 51). Khd4 and Khd5 are KHD proteins that contain 5 and 11 KHD regions, respectively. Both are more than 1,000 aa in length. Khd5 is most likely the homologue of Scp160p from *S. cerevisiae* (18, 67), since it shares substantial sequence similarity over the entire length of the protein (BLAST expect value of $9 \times e^{-42}$; Table 1). Khd6 is related to the branch point bridging protein Msl5p involved in splicing (1). According to their similarity to proteins from *S. cerevisiae*, Khd7, Khd8, and Khd9 are likely to be involved in ribosome maturation and function. Khd7 exhibits significant sequence similarity to Krr1p, a protein involved in ribosomal small subunit assembly and maintenance (55). The Khd8-related protein Pno1p is a component of the 90S preribosome involved in ribosome maturation (57). Khd9 displays high sequence similarity to the ribosomal protein S3 (Rps3p), an integral part of the small subunit of ribosomes (Fig. 1; Table 1) (66).

In order to identify DSRM proteins in *U. maydis*, we chose 29 proteins containing the DSRM: 6 from fungi and 23 from *D. melanogaster*. Only one candidate ORF, termed *dsr1*, encodes a DSRM domain (Fig. 1; Table 1). Dsr1 exhibits high sequence similarity to the mitochondrial precursor of the 60S ribosomal protein L3 from *S. cerevisiae* (Mrpl3p, Table 1) (21). Both proteins share a characteristic RNase III RIBOc domain in N-terminal proximity to the DSRM (http://smart.embl.de/). The presence of only few DSRM proteins was not surprising since *S. cerevisiae*, *S. pombe*, and *N. crassa* also contain only two each (http://smart.embl.de/). Apparently, *U. maydis* lacks a clear homologue of Rnt1p, the second DSRM protein from *S. cerevisiae* involved in small nucleolar RNA metabolism (13).

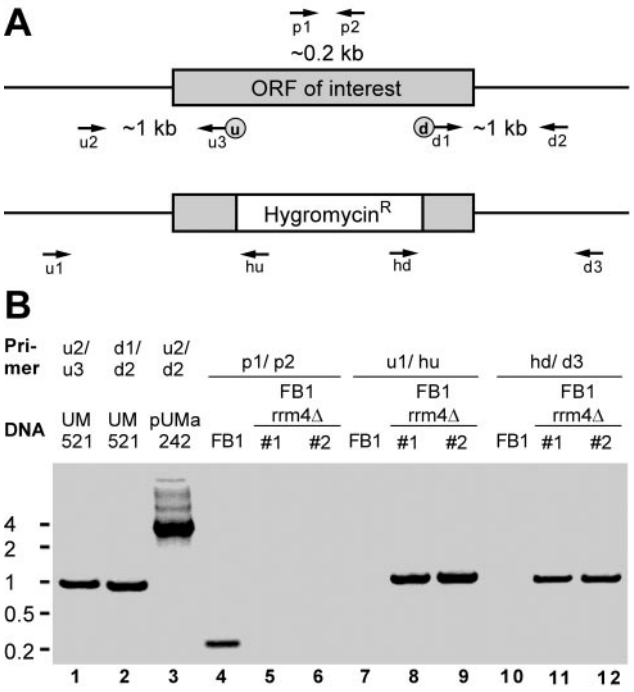

FIG. 2. Strategy to generate mutants carrying deletions in genes encoding RNA-binding proteins. (A) Schematic representation of the locus encoding the gene of interest before (above) and after (below) homologous recombination with a hygromycin resistance cassette. Labeled arrows indicate the positions of oligonucleotide primers. The locations of upstream and downstream SfiI sites are given as circled u and d, respectively. (B) Verification of successful gene replacement by PCR. As an example, strains FB1rrm4Δ#1 and -#2 are shown carrying a deletion in *rrm4*. Primer combinations and template DNA are indicated at the top. PCR products were separated on a 1.5% agarose gel and stained with ethidium bromide. Size markers are given in kilobases on the left.

To detect RRM proteins in *U. maydis*, we chose 16 RRM-containing proteins from SMART: 8 from fungi, 3 from *H. sapiens*, and 5 from *D. melanogaster*. Since the number of RRM proteins is substantially higher than the number of proteins containing the other domains (e.g., *S. cerevisiae* contains 53), we chose to list only 12 candidates (Fig. 1; Table 1). Rrm1 and Rrm5 contain two central RRM domains, while Rrm11 harbors two such motifs near the N terminus. Rrm2 exhibits a distinct domain organization consisting of an RRM domain adjacent to a SWAP (suppressor-of-white-apricot splicing regulator) domain and an RPR (regulation of pre-mRNA) domain. The latter two domains are found in proteins involved in regulation of processing nuclear pre-mRNA (http://smart.embl.de/). Proteins sharing this particular domain organization are also found in *C. elegans*, *H. sapiens*, *D. melanogaster*, and *A. thaliana* but are absent in *S. pombe* or *S. cerevisiae* (http://smart.embl.de/). Rrm12 is most likely the functional homologue of the poly(A)-binding Pab1p. It contains the characteristic domain organization of poly(A)-binding proteins from other species consisting of four N-terminal RRM domains in combination with a C-terminal PABC domain [poly(A)-binding protein C-terminal domain; Fig. 1; Table 1; BLAST expect value of e^{-132}]. Rrm4 shares a similar domain composition. However, this potential RNA-binding protein exhibits a novel domain architecture, since it contains only three N-terminal RRM domains that are combined with a C-terminal PABC domain (http://smart.embl.de/). Rrm8 contains four central RRM domains and is similar to Ylp184p from *S. cerevisiae* and to the negative regulator of development Nrd1 from *S. pombe* (64). Rrm9 carries in addition to its RRM region an R3H domain, which exhibits a characteristic spacing of conserved arginine (R) and histidine (H) residues and is implicated in binding single-stranded nucleic acids. This domain organization has not been found in proteins of the aforementioned model organisms (http://smart.embl.de). In summary, using known RNA-binding proteins as a template, we were able to identify 27 ORFs in *U. maydis* encoding 5 proteins of the PUM type, 9 of the KHD type, a single protein of the DSRM type, and 12 of the RRM type.

Phenotyping of mutants carrying deletions in genes encoding proteins of the PUM, KHD, and RRM types. In order to investigate the function of the identified ORFs, we chose a subset of 18 ORFs for a reverse genetic approach: *pum1* to *-3*, *khd1* to *-4*, and *rrm1* to *-11* (Tables 1 and 2). We focused on those genes that were not highly similar in sequence to essential genes from *S. cerevisiae*. Therefore, proteins such as Khd6 to Khd9, potentially involved in ribosomal processes, or the putative poly(A)-binding protein Rrm12 were omitted (Table 1). Respective gene replacement mutants were obtained by a PCR-based approach (Materials and Methods; Table 2 and Fig. 2) (10, 28). For each gene, two independent deletion strains were generated in strain FB1 as well as FB2 (*a1b1* and *a2b2*, respectively; Table 2).

All deletion strains were viable and were subjected to a detailed phenotypic analysis assaying morphology and pigmentation of colonies, growth on solid minimal medium at various temperatures, doubling time in liquid medium, cell morphology, cAMP-dependent cell aggregation, mating on plates containing activated charcoal, as well as disease symptoms on corn seedlings (Materials and Methods) (Tables 3 and 4). None of the deletions caused auxotrophy, heat sensitivity, abnormal morphology, or pigmentation of colonies (Table 3). To score the cAMP response, deletion strains were grown in the presence of 15 mM cAMP (Materials and Methods). Wild-type strains respond to the presence of external cAMP with a characteristic cell separation defect resulting in cell aggregates (Materials and Methods) (20, 33). Only *khd4*Δ strains differed from the wild type by containing a large proportion of cell aggregates in the absence of external cAMP. This phenotype was not enhanced by cAMP addition (see Fig. S2 in the supplemental material).

Assaying deletion strains for cold sensitivity, growth rate, morphology, mating, and pathogenicity revealed mutant phenotypes in the cases of the *khd1*Δ, *khd4*Δ, and *rrm4*Δ strains (Tables 3 and 4). In comparison to the wild type, all *khd1*Δ strains were reduced in growth at 15°C on plates as well as in liquid culture, indicating a cold-sensitive growth phenotype (Table 3) (data not shown). *khd4*Δ and *rrm4*Δ strains were disturbed in mating and pathogenicity. In addition, *khd4*Δ strains differed from the wild type in growth rate and cell morphology (Table 3).

***khd4*Δ strains are affected in growth, pheromone response, filamentation, and cell morphology, as well as pathogenicity.** Analysis of *khd4*Δ strains revealed a number of aberrant phe-

TABLE 2. Deletion of genes encoding RNA-binding proteins

Gene	Size (bp) of:			Replacement strain generated with primer[a]:								pUMa plasmid no.	UMa deletion strain no.	
	Flanking region		Diagnostic PCR product											
	Upstream	Downstream		u1	u2	u3	d1	d2	d3	p1	p2		*a1b1*	*a2b2*
pum1	931	1,085	272	MF123	MF124	MF125	MF142	MF127	MF128	MF181	MF182	215	123	124
pum2	1,055	1,000	199	MF129	MF130	MF131	MF132	MF133	MF134	MF183	MF184	216	121	122
pum3	1,011	1,056	225	MF135	MF136	MF137	MF138	MF139	MF140	MF185	MF186	217	125	126
khd1	880	829	248	MF149	MF150	MF151	MF152	MF153	MF154	MF229	MF230	233	127	128
khd2	991	1,021	328	MF143	MF144	MF145	MF146	MF147	MF148	MF227	MF228	234	139	140
khd3	867	966	230	MF155	MF156	MF157	MF158	MF159	MF160	MF231	MF232	235	137	138
khd4	853	917	257	MF161	MF162	MF163	MF164	MF165	MF166	MF233	MF234	236[b]	163	160
rrm1	888	998	181	MF302	MF303	MF304	MF305	MF306	MF307	MF308	MF309	248	175	176
rrm2	907	908	247	MF318	MF319	MF320	MF321	MF322	MF323	MF324	MF325	249	177	178
rrm3	809	849	356	MF211	MF212	MF213	MF214	MF215	MF216	MF217	MF218	241	211	210
rrm4	1,049	942	265	MF219	MF220	MF221	MF222	MF223	MF224	MF225	MF226	242[c]	170	171
rrm5	839	823	258	MF237	MF238	MF239	MF240	MF241	MF242	MF243	MF244	243	146	145
rrm6	910	834	192	MF245	MF246	MF247	MF248	MF249	MF250	MF251	MF252	283	173	174
rrm7	765	905	219	MF253	MF254	MF255	MF256	MF257	MF258	MF259	MF260	246	153	162
rrm8	780	919	219	MF326	MF327	MF328	MF329	MF330	MF331	MF332	MF333	289	165	166
rrm9	995	767	236	MF269	MF270	MF271	MF272	MF273	MF274	MF426	MF427	238	154	172
rrm10	903	899	203	MF277	MF278	MF279	MF280	MF281	MF282	MF283	MF284	245	152	161
rrm11	775	871	259	MF334	MF335	MF336	MF337	MF338	MF339	MF340	MF341	253	199	200

[a] The sequence of the oligonucleotide primers is given in Table S1 in the supplemental material.
[b] This plasmid was also used to generate UMa205#1 and -#2 (*a1mfa2bE1bW2, khd4*Δ), using SG200 as a progenitor.
[c] This plasmid was used to generate UMa212#1 and -#2 (*a1mfa2bE1bW2, rrm4*Δ), using SG200 as a progenitor.

notypes. First, mutants showed a twofold longer doubling time of 330 min with respect to wild-type strains (Materials and Methods) (see Fig. S1 in the supplemental material). Second, mating assays on activated charcoal-containing plates revealed an almost complete absence of dikaryotic hyphae in crosses of compatible *khd4* deletion strains and a significant reduction when *khd4*Δ strains were cospotted with wild-type strains, indicative of defects in pheromone response and filamentation (Fig. 3A). Third, to test whether pheromone secretion was disturbed in *khd4*Δ strains, serial dilutions were cospotted with the diploid pheromone tester strain FBD12-17 (*a2a2b1b2*) on plates containing activated charcoal. In response to a1 pheromone, FBD12-17 switches to filament formation without prior cell fusion (5). *khd4* deletion mutants were significantly reduced in elicitation of filament formation in FBD12-17, indicating reduced pheromone production (Fig. 3B). Fourth, to assay conjugation tube formation, wild-type as well as *khd4*Δ strains were incubated for 6 h in liquid CM with synthetic a1 or a2 pheromone (Materials and Methods) (62). Untreated *khd4*Δ cells were defective in cytokinesis, often shaped like lemons or droplets, and showed an increased diameter with respect to the wild type (Fig. 3C). Upon pheromone stimulation, only a few *khd4*Δ cells responded by formation of conjugation tubes, and these were substantially shorter and thicker than the wild type (Fig. 3C).

Fifth, to assay the effects of Khd4 on *b*-dependent filamentation, *khd4* was deleted in strain SG200 (*a1mfa2bE1bW2*). This strain grows filamentously on activated charcoal-containing plates, because autocrine pheromone stimulation triggers expression of an active bE1/bW2 heterodimer (8). SG200 strains carrying a deletion in *khd4* exhibited a substantially decreased capability to form filaments on activated charcoal-containing plates compared to SG200 (Fig. 3D).

Sixth, to test for virulence of *khd4*Δ strains, 7-day-old corn seedlings were infected with a cross of compatible deletion strains (Materials and Methods). Formation of tumors was scored after 2 weeks and compared to that of the wild type. Mixtures of FB1khd4Δ#1 with FB2khd4Δ#1 and FB1khd4Δ#2 with FB2khd4Δ#2 showed 16 and 27% tumor formation, respectively. This was approximately fourfold lower than the tumor formation of a mixture of wild-type strains (80% tumor formation in FB1 × FB2 crosses; Table 4). In summary, loss of Khd4 results in reduced pheromone secretion, conjugation tube formation, and *b*-dependent filamentation, as well as pathogenicity.

***rrm4*Δ strains are reduced in filamentous growth and virulence.** According to our initial phenotypic analysis, *rrm4*Δ strains were slightly affected in mating (Table 3). Since the mating defects were only subtle, we performed more elaborate assays. Cospotting of strain FB2rrm4Δ#1 with serial dilutions of either FB1 (*a1b1*) or FB1rrm4Δ#1 on activated charcoal-containing plates confirmed that *rrm4* deletion strains were impaired in mating (Fig. 4A, top), which could be due to defects in *a*-dependent pheromone response or in *b*-dependent filamentation. To test pheromone response, respective strains were cospotted in serial dilutions with diploid pheromone tester strain FBD12-17 (*a2a2b1b2*) (5). We observed no difference between elicitation of pheromone-induced filamentation of the diploid tester strain by either the wild type or FB1rrm4Δ#1 (Fig. 4B). We also tested conjugation tube formation by treatment of FB1rrm4Δ#1/#2 or FB2rrm4Δ#1/#2 with synthetic a1 or a2 pheromone (62) and could not observe any difference from the wild type (data not shown). To assay for postfusion defects in filament formation, we addressed whether wild-type strains were able to complement the mating defect of *rrm4*Δ strains. Therefore, we cospotted FB2 (*a2b2*) with serial dilutions of either FB1 (*a1b1*) or FB1rrm4Δ#1. The observation that there was no difference between the wild type and FB1rrm4Δ#1 (Fig. 4C) indicated that wild-type strains are

TABLE 3. Phenotyping of strains carrying deletions in genes encoding proteins of the PUM, KHD, or RRM type

Gene	Morphology and pigmentation of colonies[a]	Growth on plates				Doubling time[b]	Cell morphology[c]	cAMP response[d]	Mating[e]	Pathogenicity[f]
		CM at 28°C	NM							
			28°C	15°C	34°C					
pum1	wt	wt	wt	wt	wt	wt	wt	wt	wt	wt
pum2	wt	wt	wt	wt	wt	wt	wt	wt	wt	wt
pum3	wt	wt	wt	wt	wt	wt	wt	wt	wt	wt
khd1	wt	wt	wt	Cold sensitive	wt	wt	wt	wt	wt	wt
khd2	wt	wt	wt	wt	wt	wt	wt	wt	wt	wt
khd3	wt	wt	wt	wt	wt	wt	wt	wt	wt	wt
khd4	wt	wt	wt	wt	wt	Increased	Aberrant	Aberrant	Reduced	Reduced
rrm1	wt	wt	wt	wt	wt	wt	wt	wt	wt	wt
rrm2	wt	wt	wt	wt	wt	wt	wt	wt	wt	wt
rrm3	wt	wt	wt	wt	wt	wt	wt	wt	wt	wt
rrm4	wt	wt	wt	wt	wt	wt	wt	wt	Reduced	Reduced[g]
rrm5	wt	wt	wt	wt	wt	wt	wt	wt	wt	wt
rrm6	wt	wt	wt	wt	wt	wt	wt	wt	wt	wt
rrm7	wt	wt	wt	wt	wt	wt	wt	wt	wt	wt
rrm8	wt	wt	wt	wt	wt	wt	wt	wt	wt	wt
rrm9	wt	wt	wt	wt	wt	wt	wt	wt	wt	wt
rrm10	wt	wt	wt	wt	wt	wt	wt	wt	wt	wt
rrm11	wt	wt	wt	wt	wt	wt	wt	wt	wt	wt

[a] Morphology and pigmentation were scored on CM and nitrate minimal medium plates (Materials and Methods). wt, comparable to wild type.
[b] Doubling time was measured during exponential growth of strains in liquid CM (see Fig. S1 in the supplemental material).
[c] Cell morphology was determined by differential interference contrast light microscopy of cells grown in liquid CM.
[d] cAMP response was analyzed by quantifying the cytokinesis defect of strains grown in the presence of 15 mM cAMP (see Fig. S2 in the supplemental material).
[e] Mating was investigated by cospotting of compatible haploid deletion strains on plates containing activated charcoal.
[f] Pathogenicity was determined by infection of corn seedlings with mixtures of compatible deletion strains (Table 4).
[g] Pathogenicity was scored with a more detailed disease rating (Fig. 5B).

able to rescue the mating defect of *rrm4*Δ strains, suggesting a role for Rrm4 in postfusion events. For verification, we deleted *rrm4* in strain SG200 (*a1mfa2bW2bE1*) (8). SG200rrm4Δ#1 and -#2 strains produced only short filaments compared to the SG200 progenitor (Fig. 4D). These data illustrate that Rrm4 is not drastically affected in pheromone response but is crucial for *b*-dependent filamentation.

To assay pathogenicity, compatible *rrm4*Δ strains were mixed (FB1rrm4Δ#1 with FB2rrm4Δ#1 and FB1rrm4Δ#2 with FB2rrm4Δ#2) and more than 360 corn seedlings each were infected in five independent infection experiments (Materials and Methods; Fig. 5B). We observed that, in mixtures of *rrm4*Δ strains, the number of wilted or dead plants decreased approximately 1 order of magnitude in comparison to the wild type, whereas the number of plants without symptoms or with minor leaf tumors increased approximately threefold (Fig. 5B). Thus, *rrm4*Δ strains are still able to form tumors, but virulence is strongly affected.

DISCUSSION

Research on RNA-binding proteins in filamentous fungi is still in its infancy, and only a few examples of their biological roles exist (53, 65), such as regulation of *areA* mRNA stability by nitrogen metabolite signaling in *Aspergillus nidulans* (43, 50) or translational regulation by small upstream ORFs in *arg-2* and *cpcA* mRNA from *N. crassa* and *A. nidulans*, respectively (19, 23). Here, we addressed the roles of the PUM-, KHD-, and RRM-type RNA-binding proteins in *U. maydis*, through an approach that combined bioinformatics with reverse genetics. A substantial part of our study is a detailed phenotyping

TABLE 4. Pathogenicity of strains with genes encoding RNA-binding proteins deleted

Gene	No. of seedlings				% with tumors		No. of seedlings (wild type)[c]		% with tumors (wild type)[c]
	Infected[a]		With tumors				Infected	With tumors	
	#1	#2	#1	#2	#1	#2			
pum1	59	55	57	48	97	87	58	52	90
pum2	57	58	54	54	95	93	58	52	90
pum3	54	50	52	44	96	88	52	43	83
khd1	78	57	70	45	90	79	109	99	91
khd2	59	58	54	55	92	95	66	61	92
khd3	59	65	56	63	95	97	66	61	92
khd4	73	67	12	18	16	27	78	62	79
rrm1	67	57	56	51	84	89	66	62	94
rrm2	80	71	77	63	96	89	80	73	91
rrm3	60	56	58	56	97	100	54	54	100
rrm4	—[b]	—[b]	—	—	—	—	—	—	—
rrm5	70	46	60	45	86	98	107	96	90
rrm6	65	58	58	53	99	91	99	89	90
rrm7	50	46	47	43	94	93	47	47	100
rrm8	80	74	72	61	90	82	75	64	85
rrm9	45	46	39	41	87	89	57	45	79
rrm10	51	46	47	37	92	80	57	45	79
rrm11	64	55	48	40	75	73	99	81	82

[a] Crossings of two compatible deletion strains: e.g., FB1khd4Δ#1 × FB2khd4Δ#1 or FB1khd4Δ#2 × FB2khd4Δ#2.
[b] —, pathogenicity of *rrm4*Δ strains was scored with a more elaborate disease rating (Fig. 5B).
[c] Crossings of two compatible wild-type strains FB1 × FB2 were carried out in parallel to validate the infection rate; identical numbers indicate experiments in parallel.

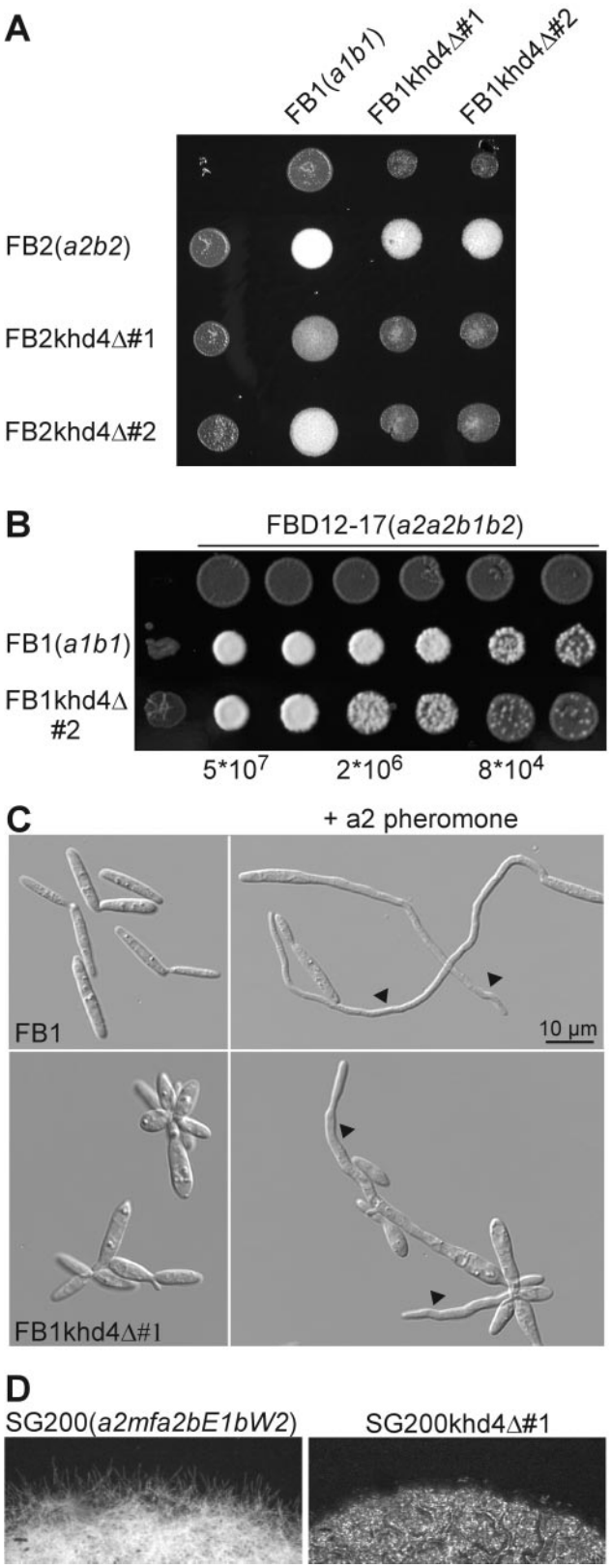

FIG. 3. *khd4*Δ strains are impaired in mating and morphology. (A) Strains indicated on the left were coinoculated on activated charcoal-containing plates. The strains are indicated at the top. Successful mating events can be scored as the amount of aerial hyphae resulting in white, fuzzy colonies. (B) Serial fivefold dilutions (given at the bottom) of strains indicated on the left were cospotted with diploid pheromone tester strain FBD12-17 (*a2a2b1b2*; 5×10^7 cells/ml; top). Pheromone secretion is direct proportional to filamentation of the pheromone tester strain. (C) Formation of conjugation tubes (arrowheads) was observed by differential interference contrast light microscopy. FB1 (*a1b1*; top) or FB1kdh4Δ#1 (bottom) was incubated in the absence (left) or presence (right) of compatible synthetic a2 pheromone (top) (62) for 5 h in liquid CM. (D) The strains indicated at the top were grown on plates containing activated charcoal. Formation of filaments was visible at the edge of the colony. These strains grew filamentously on plates containing activated charcoal due to autocrine stimulation of pheromone-induced expression of compatible bE/bW transcription factors.

regimen custom tailored for the biology of this fungus. To our knowledge, this is the first example of an extensive reverse genetic approach in filamentous fungi since the postgenomic era has been launched. We succeeded in the identification of two RNA-binding proteins implicated in pathogenic development: a KHD protein that belongs to a novel family of KHD proteins and a so far unique ELAV (embryonic lethal abnormal vision)-like RRM protein.

RNA-binding proteins of the PUM type in *U. maydis*. *U. maydis* contains five PUM-type proteins, and it is very likely that these are all members of this particular family, since the primary sequence and iterative nature of Pumilio-like repeats are very conserved (70). This notion is supported by a phylogenetic analysis of fungal PUM-type proteins. Representatives from *U. maydis* are present in all four clusters and in an additional region of nonclustering sequences. All five proteins fall into separate branches of the dendrogram, indicating that they did not arise by recent gene duplication. This is likely the case for other proteins such as Puf1p and Puf2p from *S. cerevisiae* (Fig. 6A).

Our phenotypic analysis of *pum1* to *-3* deletion strains revealed no difference from wild-type strains. The fact that PUM protein-encoding genes are not essential for viability is consistent with previous work in *S. cerevisiae*. There, it was demonstrated that deletion mutants of each of the five PUM-type proteins as well as a corresponding quintuple-deletion mutant were viable at temperatures ranging from 18 to 37°C (48). However, the observation that none of the tested deletion strains was affected in mating, cAMP response, or pathogenicity was surprising since connections between pheromone response and cAMP signaling have been reported for PUM-type proteins. For example, loss of Puf5p/Mpt5p in *S. cerevisiae* results in a temperature-sensitive growth phenotype, an increase in pheromone sensitivity, and a defect in recovery from pheromone-induced cell cycle arrest (14). PufA from *D. discoideum* has been implicated in translational control of *pkaC* mRNA encoding the catalytic subunit of PKA (60). The lack of phenotypes in our assays might be due to insufficient sensitivity, redundancy, or partly overlapping functions. This has been reported for Puf4p and Puf5p during regulation of life span in *S. cerevisiae* (30). In addition, we cannot rule out the possibility that other PUM-type proteins from *U. maydis*, such as Pum4 or Pum5, are involved in mating or cAMP signaling.

RNA-binding proteins of the KHD type in *U. maydis*. According to our analysis, nine KHD-type proteins are present in

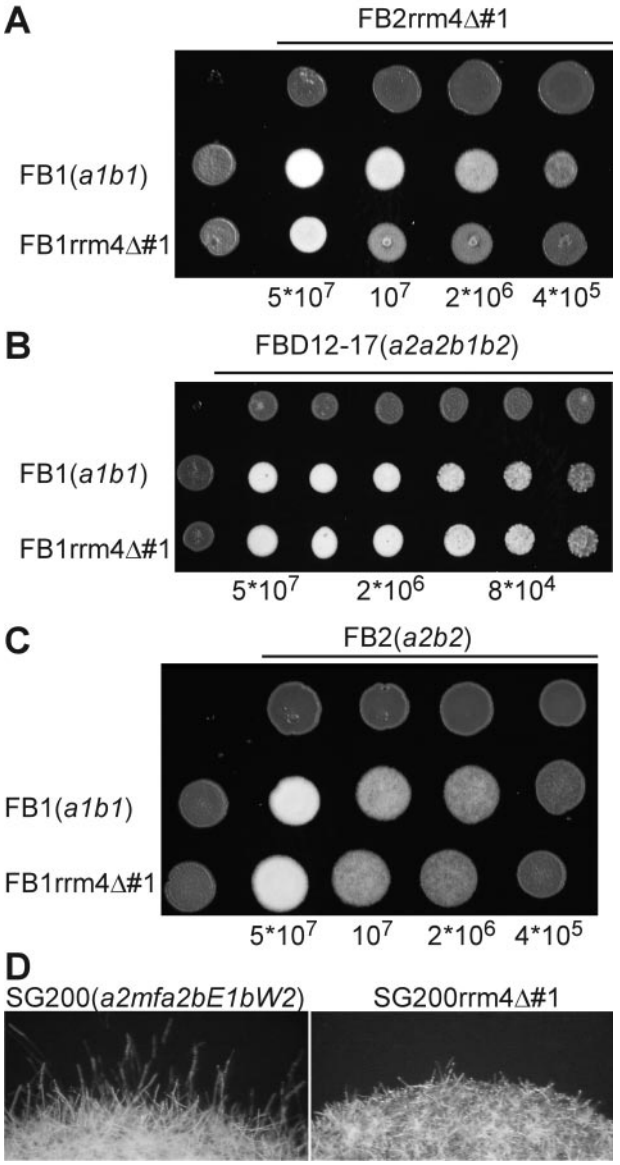

FIG. 4. *rrm4*Δ strains are impaired in filamentous growth. Strains indicated on the left were cospotted in serial fivefold dilutions (below each plate) with compatible haploid strains (A) and (C) or diploid pheromone tester strains (B; above each plate; both 5×10^7 cells/ml) on plates containing activated charcoal. Successful mating events (A) and (C) or pheromone-induced filamentation of the tester strain (B) was visible by the formation of white, fuzzy colonies. (D) The strains indicated at the top were grown on plates containing activated charcoal. Formation of filaments was visible at the edge of the colony. These strains grew filamentously on plates containing activated charcoal due to autocrine stimulation of pheromone-induced expression of active bE/bW transcription factors.

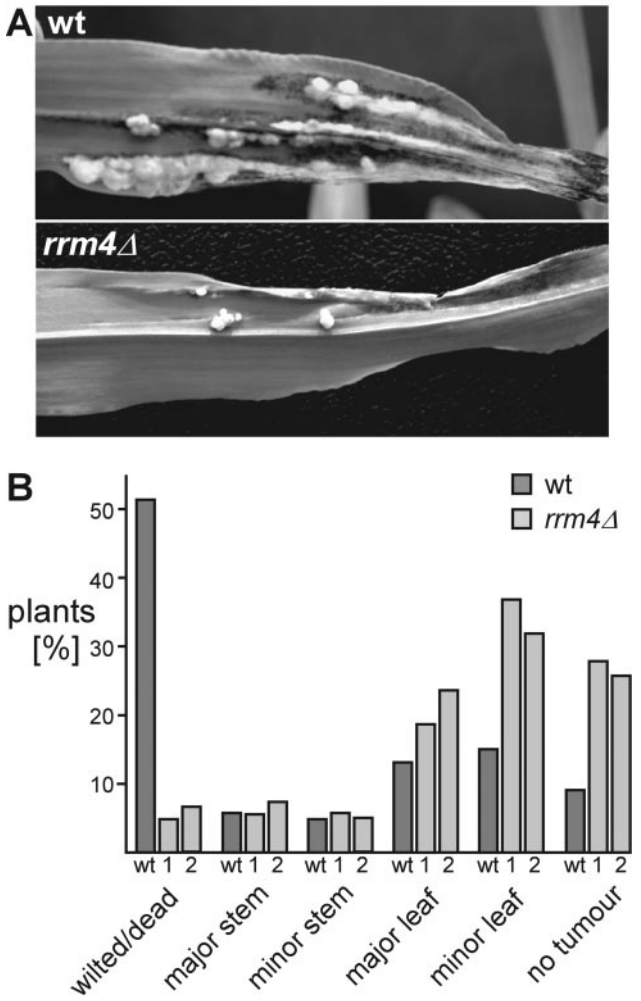

FIG. 5. *rrm4*Δ strains are reduced in virulence. Plant infection experiments were carried out by crossing either compatible wild-type (FB1 × FB2; 369 plants infected) or compatible *rrm4*Δ (FB1rrm4Δ#2 × FB2rrm4Δ#2; 368 and 403 plants infected, respectively) strains. In panel A, typical disease symptoms on leaves of corn seedlings are shown. In panel B, a detailed disease rating is given adapted from earlier work (see Materials and Methods and reference 20). The numbers of plants (percentage) that belong to the following disease categories were scored: plants with no tumor, plants with minor leaf tumors, plants with major leaf tumors, plants with minor stem tumors, plants with major stem tumors, and wilted or dead plants. The definitions for "major" and "minor" are given in Materials and Methods. The labeling below each bar indicates which mixtures of strains were tested: wt (wild type), FB1 × FB2; bars 1, FB1rrm4Δ#1 × FB2rrm4Δ#1; and bars 2, FB1rrm4Δ#2 × FB2rrm4Δ#2.

U. maydis. This number is comparable to the numbers of KHD proteins from *S. cerevisiae* and *S. pombe* (10 and 8 proteins, respectively; http://smart.embl.de/), and most of the KHD proteins from *U. maydis* have related counterparts in *S. cerevisiae* (Table 1). The phenotypic analysis of *khd1* to *-4* deletion strains revealed that *khd1*Δ strains exhibit a cold-sensitive growth phenotype, while growth of *khd2*Δ strains was not affected by temperature. This indicates that Khd1 and Khd2 have distinct biological roles, which is in accordance with the fact that the region of high sequence similarity is restricted to their three KHD RNA-binding domains (20% overall sequence identity, but the first, second, and third KHD domains are 35, 43, and 52% identical in sequence, respectively). Loss of Khd4 affected growth rate, morphology, pheromone response, filamentous growth, and pathogenicity. At present it is not clear whether these pleiotropic defects are due to altered regulation of a number of target mRNAs or whether these

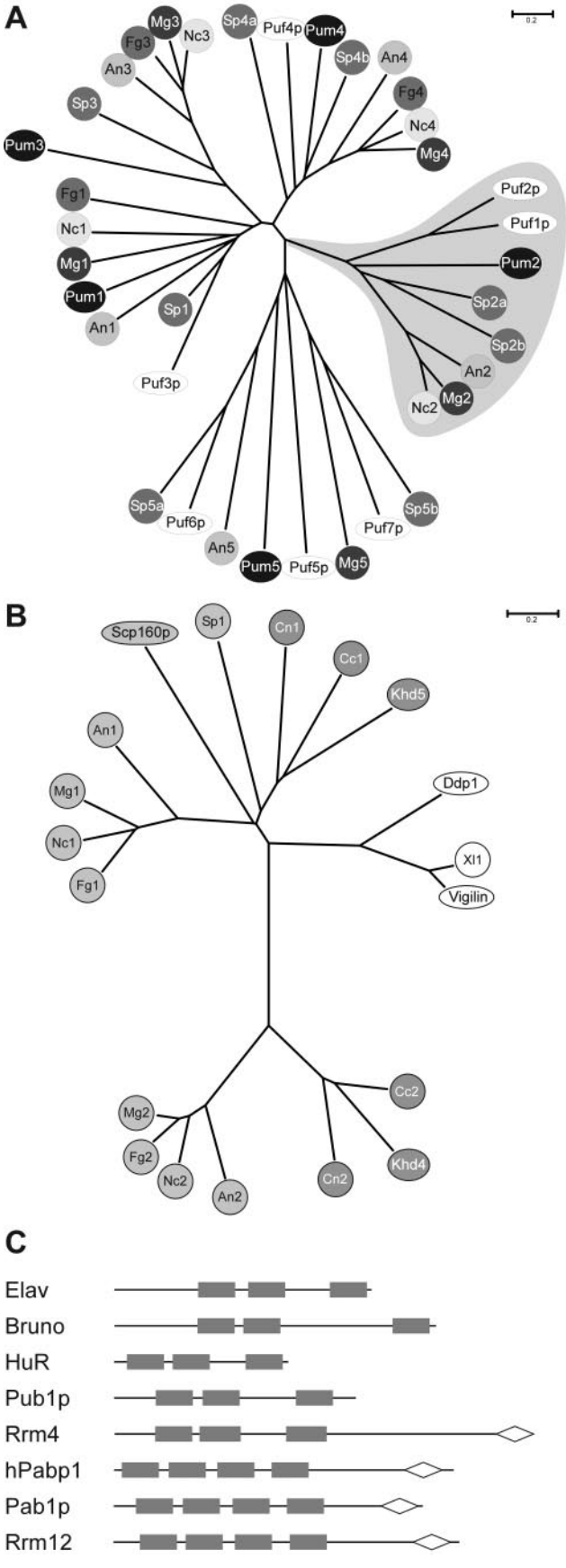

phenotypes are connected through the same key component regulated by Khd4.

Comparison to sequences from other model fungi such as *A. nidulans*, *N. crassa*, *Fusarium graminearum*, *Magnaporthe grisea*, *C. neoformans*, and *C. cinereus* revealed that Khd4 is part of a novel group of KHD proteins that are related to multi-KHD proteins of the Vigilin type. Interestingly, members of this group are absent in *S. pombe* and *S. cerevisiae* (Fig. 6B). The closest relatives from *S. cerevisiae* and mammals are the multi-KHD proteins Scp160p and Vigilin, respectively, containing 14 KHDs each. This type of protein is also found in *U. maydis* (Khd5), as well as in the other fungi mentioned above (Fig. 6B). Interestingly, loss of Scp160p from *S. cerevisiae* results in abnormal morphology (72), and recently this RNA-binding protein has been described as being involved in mating, since it interacts with the heterotrimeric G protein Gpa1p during the pheromone response (22). It will be inter-

FIG. 6. (A) PUM-type proteins in fungal model organisms. An unrooted dendrogram was created by the distance-based minimum-evolution method, based on 1,000 replicates (Materials and Methods). PUM-type protein sequences from *S. cerevisiae*, *S. pombe* (Sp), and fungi were used, whose genomes were sequenced as part of the fungal genome initiative (*A. nidulans*, An; *F. graminearum*, Fg; *M. grisea*, Mg; *N. crassa*, Nc; and *U. maydis*, Um). Proteins are either symbolized by ovals in the case of *S. cerevisiae* (Puf1p to Puf7p) and *U. maydis* (Pum1 to Pum5) or by circles with different shading in case of all other fungi. Two proteins each from *C. neoformans* (Cn) and *C. cinereus* (Cc) were omitted from the analysis because a reasonable gene prediction was not possible due to the presence of several introns. The area shaded in gray depicts PUM proteins with one or more RRMs. The accession numbers are as follows: An1, AN6587.2; An2, AN7474.2; An3, AN4285.2; An4, AN0320.2; An5, AN1235.2; Fg1, FG06710.1; Fg3, FG05203.1; Fg4, FG00841.1; Mg1, MG04985.4; Mg2, MG06318.4; Mg3, MG03158.4; Mg4, MG06982.4; Mg5, MG03872.4; Nc2, NCU06199.1; Nc3, NCU01760.1; Nc4, NCU01775.1; Puf3p (*S. cerevisiae*), Q07807; Puf2p (*S. cerevisiae*), NP_015367; Puf1p/Jsn1p (*S. cerevisiae*), P47135; Puf4p (*S. cerevisiae*), P25339; Puf5p/Mpt5p/Uth4p (*S. cerevisiae*), P39016; Puf6p (*S. cerevisiae*), Q04373; Puf7p (*S. cerevisiae*), P47077; Sp1, NP_593141; Sp2a, CAA18887; Sp2b, NP_595389; Sp3a, NP_593687; Sp3b, Q10238; Sp4a, Q09829; Sp4b, Q92359; Sp5a, NP_588564; Sp5b, Q92347; Pum2, UM00268.1; Pum3, UM05467.1; Pum4, UM03431.1; and Pum1 and Pum5, this study (Table 1). The scale bar denotes the number of substitutions per site. (B) Multi-KHD proteins in eukaryotes. An unrooted tree was derived as in panel A by aligning multi-KHD-type proteins from the same organisms as in panel A as well as *D. melanogaster* (Dm); *Xenopus laevis*, (Xl), and *H. sapiens* (Hs). Proteins are either symbolized by ovals (Scp160p, *S. cerevisiae*; Ddp1, *D. melanogaster*; Vigilin, *H. sapiens*; and Khd4, *U. maydis*) or circles. Light gray, dark gray, or open symbols indicate the origin from ascomycetes, basidiomycetes, and higher eukaryotes, respectively. Accession numbers: An1, AN2068.2; An2, AN6326.2; Ddp1 (*D. melanogaster*), CAB52798; Fg1, FG09491.1; Fg2, FG06181.1; Vigilin (*H. sapiens*), Q00341; Mg1, MG06496.4; Mg2, MG01781.4; Nc1, CAB91673; Nc2, XP_324623; Scp160p (*S. cerevisiae*), CAA46597; Sp1, NP_588106; Xl1, AAH44314; Khd4 and Khd5, this study (Table 1). The sequences of two proteins each from *C. neoformans* (Cn1 and Cn2) and *C. cinereus* (Cc1 and Cc2) were derived by conceptual translation (nucleotide positions and predicted introns are given in Materials and Methods). (C) Domain organization of ELAV-like and PABP proteins. RRM and PABC domains are given as filled rectangles and open diamonds, respectively. Accession numbers: ELAV (*D. melanogaster*), P16914; Bruno (*D. melanogaster*), AAB58464; HuR (*H. sapiens*), AAH03376; Pub1p (*S. cerevisiae*), NP014382; hPabp1 (*H. sapiens*), P11940; Pab1p, (*S. cerevisiae*), P04147; and Rrm4 and Rrm12, this study (Table 1).

esting to determine whether in *U. maydis* multi-KHD proteins such as Khd4 and Khd5 share functions in regulating morphogenesis and pheromone signaling.

RNA-binding proteins of the RRM type in *U. maydis*. An automated feature search predicted the presence of 43 RRM proteins in *U. maydis* (http://www.broad.mit.edu/cgi-bin/annotation/fungi/ustilago_maydis/findfeatures.cgi), a number that is close to the 53 RRM proteins from *S. cerevisiae* (http://smart.embl.de/). Phenotyping strains carrying a deletion in a subset of 11 RRM protein-encoding genes revealed that only the loss of Rrm4 resulted in discernible phenotypes. This was surprising since we would have expected more RRM proteins to be important for developmental processes in *U. maydis*. For example, Rrm8 shares the same domain organization as well as similar flanking sequences to the negative regulator of development Nrd1 from *S. pombe*. Loss of Nrd1 function causes cells to initiate sexual development in the absence of nutrient starvation (64). In contrast, *rrm8*Δ strains from *U. maydis* were not drastically disturbed in mating or pathogenicity.

In the case of Rrm4, we showed that neither pheromone secretion nor pheromone-responsive conjugation tube formation was significantly disturbed. However, loss of Rrm4 negatively affects dikaryotic filaments as well as filamentation of a solopathogenic strain. This defect is likely to be the cause for the reduced disease symptoms, since it is conceivable that shorter filaments have difficulties in finding an appropriate entry site for plant penetration.

Rrm4 displays a novel domain organization that is so far unique in eukaryotes (Fig. 6C). At its C terminus, it contains a PABC domain that was initially found in poly(A)-binding proteins. However, this domain is also associated with a HECT domain (homologous to the E6-AP carboxyl terminus) found in ubiquitin-protein ligases and implicated as a protein-protein interaction interface (32, 39). The PABC domain in human poly(A)-binding protein contains four amino acids (F22, I25, A33, and K35) shown to form a deep hydrophobic pocket that could function as a peptide binding domain (32). Strikingly, all four residues are conserved in Rrm4. In its N terminus, Rrm4 contains three RRM domains with typical spacing known from ELAV-like proteins (3), such as Elav or Bruno from *D. melanogaster*, HuR from *H. sapiens*, and Pub1p from *S. cerevisiae*. All of these proteins contain two RRM domains juxtaposed with each other and separated from a third by a hinge region of variable length (Fig. 6C). Members of this family of proteins have been described to function as sequence-specific RNA-binding proteins regulating mRNA translation or stability (3). For example, Bruno represses translation of Oskar, a determinant for posterior body patterning in embryos from *D. melanogaster*, by binding to Bruno response elements in the 3′-untranslated region of the *osk* mRNA (47, 68, 71). HuR from humans has been implicated in regulating AUUUA-mediated mRNA decay (16, 46). Pub1p from *S. cerevisiae* recognizes stabilizer elements and thereby protects mRNAs that contain upstream ORFs from degradation by the nonsense-mediated decay pathway (52).

According to sequence similarity, we hypothesize that Rrm4 is a sequence-specific RNA-binding protein that might be involved in regulation of mRNA splicing, transport, translation, or stability. For two reasons, we do not believe that Rrm4 functions as poly(A)-binding protein. Rrm4 does not contain the typical four RRM domains in its N terminus, and in vitro binding experiments revealed that Rrm4 does not bind to poly(A) or poly(U) but recognizes specific sequences enriched by SELEX (C. Julius and M. Feldbrügge, unpublished observation). A much better candidate for a poly(A)-binding protein in *U. maydis* is Rrm12, since it contains the characteristic domain organization (Fig. 6C) and exhibits high sequence similarity to other PABPs over its entire length (comparison to Pab1p from *S. cerevisiae* results in a BLAST expect value of e^{-132}).

Conclusions. A great surprise from our study of RNA-binding proteins in *U. maydis* was the fact that, despite our extensive phenotypic analysis, the majority of gene replacement mutants did not exhibit any discernible phenotypes. A possible explanation would be functional redundancy of related RNA-binding proteins. Alternatively, it could be possible that our assays were not sensitive enough or that we did not test the affected phenotype. Nevertheless, we were able to identify 2 out of 18 RNA-binding proteins implicated in pathogenic development of *U. maydis*. One of them is a founding member of a new group of KHD proteins, and the other is a so far unique ELAV-like RRM protein. Investigation of the subcellular localization of these candidates in combination with identification of specifically recognized target RNAs will allow us to unravel the connection between the mode of action of these RNA-binding proteins and pathogenic development. For example, nuclear localization would indicate that they function in mRNA maturation or export. We expect to find within the group of target RNAs important determinants of pathogenic development whose expression is manifested at the posttranscriptional level. The involvement of RNA-binding proteins in regulation of pathogenic development supports our initial assumption predicting fundamental similarities to developmental programs of higher eukaryotes.

ACKNOWLEDGMENTS

We acknowledge A. Brachmann, P. Müller, R. Kahmann, and STaR laboratory members for valuable discussions and critical reading of the manuscript. We thank S. Hester and J. Hohenner for excellent technical assistance. We are grateful to Julian König for generating gene replacement constructs.

This work was supported by Bayer CropScience.

REFERENCES

1. **Abovich, N., and M. Rosbash.** 1997. Cross-intron bridging interactions in the yeast commitment complex are conserved in mammals. Cell **89:**403–412.
2. **Altschul, S. F., W. Gish, W. Miller, E. W. Myers, and D. J. Lipman.** 1990. Basic local alignment search tool. J. Mol. Biol. **215:**403–410.
3. **Antic, D., and J. D. Keene.** 1997. Embryonic lethal abnormal visual RNA-binding proteins involved in growth, differentiation, and posttranscriptional gene expression. Am. J. Hum. Genet. **61:**273–278.
4. **Banuett, F.** 1995. Genetics of *Ustilago maydis*, a fungal pathogen that induces tumors in maize. Annu. Rev. Genet. **29:**179–208.
5. **Banuett, F., and I. Herskowitz.** 1989. Different *a* alleles are necessary for maintenance of filamentous growth but not for meiosis. Proc. Natl. Acad. Sci. USA **86:**5878–5882.
6. **Birney, E., S. Kumar, and A. R. Krainer.** 1993. Analysis of the RNA-recognition motif and RS and RGG domains: conservation in metazoan pre-mRNA splicing factors. Nucleic Acids Res. **21:**5803–5816.
7. **Bölker, M.** 2001. *Ustilago maydis*—a valuable model system for the study of fungal dimorphism and virulence. Microbiology **147:**1395–1401.
8. **Bölker, M., S. Genin, C. Lehmler, and R. Kahmann.** 1995. Genetic regulation of mating, and dimorphism in *Ustilago maydis*. Can. J. Bot. **73:**320–325.
9. **Bölker, M., M. Urban, and R. Kahmann.** 1992. The *a* mating type locus of *U. maydis* specifies cell signaling components. Cell **68:**441–450.
10. **Brachmann, A., J. König, C. Julius, and M. Feldbrügge.** Reverse genetic approach for generating gene replacement mutants in *Ustilago maydis.* Mol. Genet. Genomics **272:**216–226.

11. **Brachmann, A., J. Schirawski, P. Müller, and R. Kahmann.** 2003. An unusual MAP kinase is required for efficient penetration of the plant surface by *Ustilago maydis*. EMBO J. **22:**2199–2210.
12. **Burd, C. G., and G. Dreyfuss.** 1994. Conserved structures and diversity of functions of RNA-binding proteins. Science **265:**615–621.
13. **Chanfreau, G., P. Legrain, and A. Jacquier.** 1998. Yeast RNase III as a key processing enzyme in small nucleolar RNAs metabolism. J. Mol. Biol. **284:**975–988.
14. **Chen, T., and J. Kurjan.** 1997. *Saccharomyces cerevisiae* Mpt5p interacts with Sst2p and plays roles in pheromone sensitivity and recovery from pheromone arrest. Mol. Cell. Biol. **17:**3429–3439.
15. **Dreyfuss, G., V. N. Kim, and N. Kataoka.** 2002. Messenger-RNA-binding proteins and the messages they carry. Nat. Rev. Mol. Cell Biol. **3:**195–205.
16. **Fan, X. C., and J. A. Steitz.** 1998. Overexpression of HuR, a nuclear-cytoplasmic shuttling protein, increases the in vivo stability of ARE-containing mRNAs. EMBO J. **17:**3448–3460.
17. **Feldbrügge, M., J. Kämper, G. Steinberg, and R. Kahmann.** Regulation of mating and pathogenic development in *Ustilago maydis.* Curr. Opin. Microbiol. **7:**666–672.
18. **Frey, S., M. Pool, and M. Seedorf.** 2001. Scp160p, an RNA-binding, polysome-associated protein, localizes to the endoplasmic reticulum of *Saccharomyces cerevisiae* in a microtubule-dependent manner. J. Biol. Chem. **276:**15905–15912.
19. **Gaba, A., Z. Wang, T. Krishnamoorthy, A. G. Hinnebusch, and M. S. Sachs.** 2001. Physical evidence for distinct mechanisms of translational control by upstream open reading frames. EMBO J. **20:**6453–6463.
20. **Gold, S. E., S. M. Brogdon, M. E. Mayorga, and J. W. Kronstad.** 1997. The *Ustilago maydis* regulatory subunit of a cAMP-dependent protein kinase is required for gall formation in maize. Plant Cell **9:**1585–1594.
21. **Graack, H. R., L. Grohmann, M. Kitakawa, K. L. Schafer, and V. Kruft.** 1992. YmL9, a nucleus-encoded mitochondrial ribosomal protein of yeast, is homologous to L3 ribosomal proteins from all natural kingdoms and photosynthetic organelles. Eur. J. Biochem. **206:**373–380.
22. **Guo, M., C. Aston, S. A. Burchett, C. Dyke, S. Fields, S. J. Rajarao, P. Uetz, Y. Wang, K. Young, and H. G. Dohlman.** 2003. The yeast G protein alpha subunit Gpa1 transmits a signal through an RNA binding effector protein Scp160. Mol. Cell **12:**517–524.
23. **Hoffmann, B., O. Valerius, M. Andermann, and G. H. Braus.** 2001. Transcriptional autoregulation and inhibition of mRNA translation of amino acid regulator gene cpcA of filamentous fungus *Aspergillus nidulans*. Mol. Biol. Cell **12:**2846–2857.
24. **Holliday, R.** 1974. *Ustilago maydis*, p. 575–595. *In* R. C. King (ed.), Handbook of genetics, vol. 1. Plenum Press, New York, N.Y.
25. **Hull, C. M., and J. Heitman.** 2002. Genetics of *Cryptococcus neoformans*. Annu. Rev. Genet. **36:**557–615.
26. **Jeong, H. T., F. Ozoe, K. Tanaka, T. Nakagawa, H. Matsuda, and M. Kawamukai.** 2004. A novel gene, msa1, inhibits sexual differentiation in *Schizosaccharomyces pombe*. Genetics **167:**77–91.
27. **Kahmann, R., and J. Kämper.** *Ustilago maydis*: how its biology relates to pathogenic development. New Phytol. **164:**31–42.
28. **Kämper, J.** 2004. A PCR-based system for highly efficient generation of gene replacement mutants in *Ustilago maydis*. Mol. Genet. Genomics **271:**103–110.
29. **Kämper, J., M. Reichmann, T. Romeis, M. Bölker, and R. Kahmann.** 1995. Multiallelic recognition: nonself-dependent dimerization of the bE and bW homeodomain proteins in *Ustilago maydis*. Cell **81:**73–83.
30. **Kennedy, B. K., M. Gotta, D. A. Sinclair, K. Mills, D. S. McNabb, M. Murthy, S. M. Pak, T. Laroche, S. M. Gasser, and L. Guarente.** 1997. Redistribution of silencing proteins from telomeres to the nucleolus is associated with extension of life span in *S. cerevisiae*. Cell **89:**381–391.
31. **Kharrat, A., M. J. Macias, T. J. Gibson, M. Nilges, and A. Pastore.** 1995. Structure of the dsRNA binding domain of *E. coli* RNase III. EMBO J. **14:**3572–3584.
32. **Kozlov, G., J. F. Trempe, K. Khaleghpour, A. Kahvejian, I. Ekiel, and K. Gehring.** 2001. Structure and function of the C-terminal PABC domain of human poly(A)-binding protein. Proc. Natl. Acad. Sci. USA **98:**4409–4413.
33. **Krüger, J., G. Loubradou, E. Regenfelder, A. Hartmann, and R. Kahmann.** 1998. Crosstalk between cAMP and pheromone signalling pathways in *Ustilago maydis*. Mol. Gen. Genet. **260:**193–198.
34. **Kuersten, S., and E. B. Goodwin.** 2003. The power of the 3′ UTR: translational control and development. Nat. Rev. Genet. **4:**626–637.
35. **Kumar, S., K. Tamura, I. B. Jakobsen, and M. Nei.** 2001. MEGA2: molecular evolutionary genetics analysis software. Bioinformatics **17:**1244–1245.
36. **Lee, N., C. D'Souza, and J. W. Kronstad.** 2003. Of smuts, blasts, mildews, and blights: cAMP signalling in phytopathogenic fungi. Annu. Rev. Phytopathol. **41:**399–427.
37. **Letunic, I., R. R. Copley, S. Schmidt, F. D. Ciccarelli, T. Doerks, J. Schultz, C. P. Ponting, and P. Bork.** 2004. SMART 4.0: towards genomic data integration. Nucleic Acids Res. **32:**D142–D144.
38. **Lewis, H. A., K. Musunuru, K. B. Jensen, C. Edo, H. Chen, R. B. Darnell, and S. K. Burley.** 2000. Sequence-specific RNA binding by a Nova KH domain: implications for paraneoplastic disease and the fragile X syndrome. Cell **100:**323–332.
39. **Mangus, D. A., N. Amrani, and A. Jacobson.** 1998. Pbp1p, a factor interacting with *Saccharomyces cerevisiae* poly(A)-binding protein, regulates polyadenylation. Mol. Cell. Biol. **18:**7383–7396.
40. **Maniatis, T., and R. Reed.** 2002. An extensive network of coupling among gene expression machines. Nature **416:**499–506.
41. **Mattaj, I. W.** 1993. RNA recognition: a family matter? Cell **73:**837–840.
42. **Mazumder, B., V. Seshadri, and P. L. Fox.** 2003. Translational control by the 3′-UTR: the ends specify the means. Trends Biochem. Sci. **28:**91–98.
43. **Morozov, I. Y., M. G. Martinez, M. G. Jones, and M. X. Caddick.** 2000. A defined sequence within the 3′ UTR of the areA transcript is sufficient to mediate nitrogen metabolite signalling via accelerated deadenylation. Mol. Microbiol. **37:**1248–1257.
44. **Murata, Y., and R. P. Wharton.** 1995. Binding of pumilio to maternal hunchback mRNA is required for posterior patterning in Drosophila embryos. Cell **80:**747–756.
45. **Musco, G., A. Kharrat, G. Stier, F. Fraternali, T. J. Gibson, M. Nilges, and A. Pastore.** 1997. The solution structure of the first KH domain of FMR1, the protein responsible for the fragile X syndrome. Nat. Struct. Biol. **4:**712–716.
46. **Myer, V. E., X. C. Fan, and J. A. Steitz.** 1997. Identification of HuR as a protein implicated in AUUUA-mediated mRNA decay. EMBO J. **16:**2130–2139.
47. **Nakamura, A., K. Sato, and K. Hanyu-Nakamura.** 2004. Drosophila cup is an eIF4E binding protein that associates with Bruno and regulates oskar mRNA translation in oogenesis. Dev. Cell **6:**69–78.
48. **Olivas, W., and R. Parker.** 2000. The Puf3 protein is a transcript-specific regulator of mRNA degradation in yeast. EMBO J. **19:**6602–6611.
49. **Perez-Canadillas, J. M., and G. Varani.** 2001. Recent advances in RNA-protein recognition. Curr. Opin. Struct. Biol. **11:**53–58.
50. **Platt, A., T. Langdon, H. N. Arst, Jr., D. Kirk, D. Tollervey, J. M. Sanchez, and M. X. Caddick.** 1996. Nitrogen metabolite signalling involves the C-terminus and the GATA domain of the Aspergillus transcription factor AREA and the 3′ untranslated region of its mRNA. EMBO J. **15:**2791–2801.
51. **Rabitsch, K. P., A. Toth, M. Galova, A. Schleiffer, G. Schaffner, E. Aigner, C. Rupp, A. M. Penkner, A. C. Moreno-Borchart, M. Primig, R. E. Esposito, F. Klein, M. Knop, and K. Nasmyth.** 2001. A screen for genes required for meiosis and spore formation based on whole-genome expression. Curr. Biol. **11:**1001–1009.
52. **Ruiz-Echevarria, M. J., and S. W. Peltz.** 2000. The RNA binding protein Pub1 modulates the stability of transcripts containing upstream open reading frames. Cell **101:**741–751.
53. **Sachs, M. S.** 1998. Posttranscriptional control of gene expression in filamentous fungi. Fungal Genet. Biol. **23:**117–124.
54. **Sánchez-Martínez, C., and J. Pérez-Martín.** 2001. Dimorphism in fungal pathogens: *Candida albicans* and *Ustilago maydis*—similar inputs, different outputs. Curr. Opin. Microbiol. **4:**214–221.
55. **Sasaki, T., A. Toh-E, and Y. Kikuchi.** 2000. Yeast Krr1p physically and functionally interacts with a novel essential Kri1p, and both proteins are required for 40S ribosome biogenesis in the nucleolus. Mol. Cell. Biol. **20:**7971–7979.
56. **Schultz, J., F. Milpetz, P. Bork, and C. P. Ponting.** 1998. SMART, a simple modular architecture research tool: identification of signaling domains. Proc. Natl. Acad. Sci. USA **95:**5857–5864.
57. **Senapin, S., G. D. Clark-Walker, X. J. Chen, B. Seraphin, and M. C. Daugeron.** 2003. RRP20, a component of the 90S preribosome, is required for pre-18S rRNA processing in *Saccharomyces cerevisiae*. Nucleic Acids Res. **31:**2524–2533.
58. **Siomi, H., M. J. Matunis, W. M. Michael, and G. Dreyfuss.** 1993. The pre-mRNA binding K protein contains a novel evolutionarily conserved motif. Nucleic Acids Res. **21:**1193–1198.
59. **Snetselaar, K. M., M. Bölker, and R. Kahmann.** 1996. *Ustilago maydis* mating hyphae orient their growth toward pheromone sources. Fungal Genet. Biol. **20:**299–312.
60. **Souza, G. M., A. M. da Silva, and A. Kuspa.** 1999. Starvation promotes Dictyostelium development by relieving PufA inhibition of PKA translation through the YakA kinase pathway. Development **126:**3263–3274.
61. **St Johnston, D., N. H. Brown, J. G. Gall, and M. Jantsch.** 1992. A conserved double-stranded RNA-binding domain. Proc. Natl. Acad. Sci. USA **89:**10979–10983.
62. **Szabó, Z., M. Tönnis, H. Kessler, and M. Feldbrügge.** 2002. Structure-function analysis of lipopeptide pheromones from the plant pathogen *Ustilago maydis*. Mol. Genet. Genomics **268:**362–370.
63. **Thompson, J. D., T. J. Gibson, F. Plewniak, F. Jeanmougin, and D. G. Higgins.** 1997. The CLUSTAL_X windows interface: flexible strategies for multiple sequence alignment aided by quality analysis tools. Nucleic Acids Res. **25:**4876–4882.
64. **Tsukahara, K., H. Yamamoto, and H. Okayama.** 1998. An RNA binding protein negatively controlling differentiation in fission yeast. Mol. Cell. Biol. **18:**4488–4498.
65. **Vilela, C., and J. E. McCarthy.** 2003. Regulation of fungal gene expression

via short open reading frames in the mRNA 5′untranslated region. Mol. Microbiol. **49:**859–867.

66. **Warner, J. R., and C. Gorenstein.** 1978. The ribosomal proteins of *Saccharomyces cerevisiae*. Methods Cell Biol. **20:**45–60.
67. **Weber, V., A. Wernitznig, G. Hager, M. Harata, P. Frank, and U. Wintersberger.** 1997. Purification and nucleic-acid-binding properties of a *Saccharomyces cerevisiae* protein involved in the control of ploidy. Eur. J. Biochem. **249:**309–317.
68. **Webster, P. J., L. Liang, C. A. Berg, P. Lasko, and P. M. Macdonald.** 1997. Translational repressor bruno plays multiple roles in development and is widely conserved. Genes Dev. **11:**2510–2521.
69. **Wharton, R. P., J. Sonoda, T. Lee, M. Patterson, and Y. Murata.** 1998. The Pumilio RNA-binding domain is also a translational regulator. Mol. Cell **1:**863–872.
70. **Wickens, M., D. S. Bernstein, J. Kimble, and R. Parker.** 2002. A PUF family portrait: 3′UTR regulation as a way of life. Trends Genet. **18:**150–157.
71. **Wilhelm, J. E., M. Hilton, Q. Amos, and W. J. Henzel.** 2003. Cup is an eIF4E binding protein required for both the translational repression of oskar and the recruitment of Barentsz. J. Cell Biol. **163:**1197–1204.
72. **Wintersberger, U., C. Kuhne, and A. Karwan.** 1995. Scp160p, a new yeast protein associated with the nuclear membrane and the endoplasmic reticulum, is necessary for maintenance of exact ploidy. Yeast **11:**929–944.
73. **Zamore, P. D., J. R. Williamson, and R. Lehmann.** 1997. The Pumilio protein binds RNA through a conserved domain that defines a new class of RNA-binding proteins. RNA **3:**1421–1433.